THE AMERICAN SOCIETY OF MECHANICAL ENGINEERS
Three Park Avenue, New York, N.Y. 10016-5990

99-GT-350




# Effects of Alloy Composition on the Performance of Yttria Stabilized Zirconia – Thermal Barrier Coatings

**Josh Kimmel, Zaher Mutasim and William Brentnall**
Solar Turbines Incorporated
San Diego, California USA

## ABSTRACT

Thermal barrier coatings (TBCs) provide an alloy surface temperature reduction when applied to turbine component surfaces. Thermal barrier coatings can be used as a tool for the designer to augment the power and/or enhance the efficiency of gas turbine engines. TBCs have been used successfully in the aerospace industry for many years, with only limited use for industrial gas turbine applications. Industrial gas turbines operate for substantially longer cycles and time between overhauls, and thus endurance becomes a critical factor. There are many factors that affect the life of a TBC including the composition and microstructure of the base alloy and bond coating. Alloys such as Mar-M 247, CMSX-4 and CMSX-10 are materials used for high temperature turbine environments, and usually require protective and/or thermal barrier coatings for increased performance. Elements such as hafnium, rhenium, and yttrium have shown considerable improvements in the strength of these alloys. However these elements may result in varying effects on the coatability and environmental performance of these alloys. This paper discusses the effects of these elements on the performance of thermal barrier coatings.

## BACKGROUND

The demand for increased gas turbine efficiency and improved durability, while reducing life cycle cost, has evoked a lot of attention from the gas turbine original equipment manufacturers (OEMs) and end users. While OEMs are continuing their drive to improve engine performance by introducing new concepts to engine designs, there are many limitations and challenges that the engine designer experiences. These include the levels of mechanical and thermal stresses that the turbine components will experience.

The performance and durability of the industrial gas turbines are strongly dependent on the operating conditions and the environment in which they function. Advances in materials have progressed at an increasing rate over the last twenty years and as a result new superalloys have emerged to support the new challenging demands and requirements of gas turbines. The evolution of directionally solidified (DS) and single crystal (SX) alloys has resulted in higher temperature creep and fatigue strengths. These improved properties resulted from the addition of refractory elements such as tungsten and rhenium and the implementation of uni-directional and single crystal manufacturing processes. A metal temperature capability improvement of 25°F is achieved with a change from equiaxed to a directionally solidified CM 247 LC alloy, and an additional 30-40°F could be achieved with the use of a single crystal version of the same alloy (Erickson, 1995). Additional temperature gains are achieved by additions of rhenium. This performance improvement could be achieved, but at the expense of the alloy environmental resistance properties. The use of improved cooling schemes and DS or single crystal alloys to raise the temperature capability, is very close to reaching its limit. Thermal barrier coatings (TBCs) are the next step to achieve further temperature gains, or as an alternative to higher cost DS or single crystal alloys. TBCs are used to reduce the surface metal temperature to workable ranges.

A thermal barrier coating consists of a bond coating applied directly to the alloy, and a ceramic top coat applied to the bond coating. The bond coating is an oxidation resistant coating such as a diffusion platinum aluminide or a MCrAlY coating. The function of the metallic bond coating is to provide oxidation protection to the metallic substrate, minimize the thermal expansion mismatch and provide strain compliance between the substrate and the ceramic layer (Brindley and Miller, 1989). The ceramic layer with low thermal conductivity creates a thermal gradient needed across the TBC system. The ceramic coating most commonly used in industry is a 7-8 wt.% yttria stabilized zirconia (YSZ), due to the combination of low thermal conductivity and a thermal expansion close to nickel base superalloys.

There is a tremendous amount of experience using TBCs in aerospace engines (Maricocchi, et.al., 1995; Bose and DeMasi, 1995). Unfortunately, there is limited TBC experience in industrial gas turbine environments (Mutasim, et.al., 1997; Mutasim and Brentnall, 1995; Nelson and Orenstein, 1995), which show substantially different conditions. Industrial gas turbines (IGT) operate for substantially longer cycles and times between overhauls, and thus endurance becomes a critical factor. Table 1 shows the TBC requirements for aircraft and IGT environments. It is clear that industrial gas turbine users need to

Presented at the International Gas Turbine & Aeroengine Congress & Exhibition
Indianapolis, Indiana — June 7–June 10, 1999
This paper has been accepted for publication in the Transactions of the ASME
Discussion of it will be accepted at ASME Headquarters until September 30, 1999

**Table 1 – Aircraft and IGT Gas Turbines TBC Requirements**

| Requirement | Aircraft | IGT |
|---|---|---|
| Service Time (Hours) | 8000 | 30,000 |
| Number of Cycles | 1000 – 8000 | 10 – 3000 |
| Peak Surface Temperature (°F) | >2300 | <2000 |
| Environment | Oxidative / Erosive | Oxidative / Corrosive |

gain laboratory and engine experience to determine if TBCs can be used as a prime-reliant coating.

This paper discusses the performance of electron beam-physical vapor deposited (EB-PVD), and air plasma sprayed (APS) TBCs on three nickel base superalloys: equiaxed Mar-M247, single crystal CMSX-4, and the new third-generation single crystal CMSX-10 alloy. CMSX-10 alloy is of great interest to the gas turbine industry because of its improved mechanical properties at high temperatures. The effects of temperature, cycle time, and alloy selection on TBC performance will be discussed along with the associated failure mechanisms.

## PROCESSING

Mar-M 247, CMSX-4, and CMSX-10 nickel base superalloy buttons (1" diameter x 0.125" thick) were coated with EB-PVD and air plasma spray TBC systems. The EB-PVD bond coat consisted of a single-phase platinum aluminide bond coating applied by platinum electroplating followed by above-the-pack aluminizing. The 6-8 wt.% yttria stabilized zirconia TBC was applied using EB-PVD TBC processing. The APS system consisted of a Co-32Ni-22Cr-12Al-0.75Y-1.5Si bond coating, and a 6-8 wt.% YSZ-TBC top coating. Processing conditions for the coated specimens included surface preparation by grit blasting, heat treating the bond coating to improve its surface finish and adherence for EB-PVD only, and final heat treatments as required per substrate alloy requirements.

## TESTING

Coated specimens were evaluated for coating microstructure and composition using a scanning electron microscope (SEM) equipped with energy dispersive X-ray (EDX) analyzer. Thermal cycle testing at 2000°F (100 hour cycles), 2000°F (10 hour cycles), and 1900°F (100 hour cycles) were conducted in a still-air conduction furnace using duplicate specimens. The metallographic preparation procedure included mounting the specimens in epoxy resin containers prior to sectioning to minimize cracking during subsequent sectioning and polishing.

## RESULTS

### As-Coated

**Microstructure**. Figure 1 is a scanning electron micrograph that displays the above-the-pack PtAl bond coat and EB-PVD TBC top coat microstructure on CMSX-4 alloy. The platinum aluminide bond coat consists of a single phase, two-layer coating as displayed in Figure 1, where the outer 35 microns layer consists of a single-phase platinum rich beta NiAl matrix. The second layer is a 35 micron thick refractory enriched diffusion zone that is located at the interface. The coating displays a high content of dark inclusions at the center of the coating. The inclusions were identified as alumina grit particles that were used

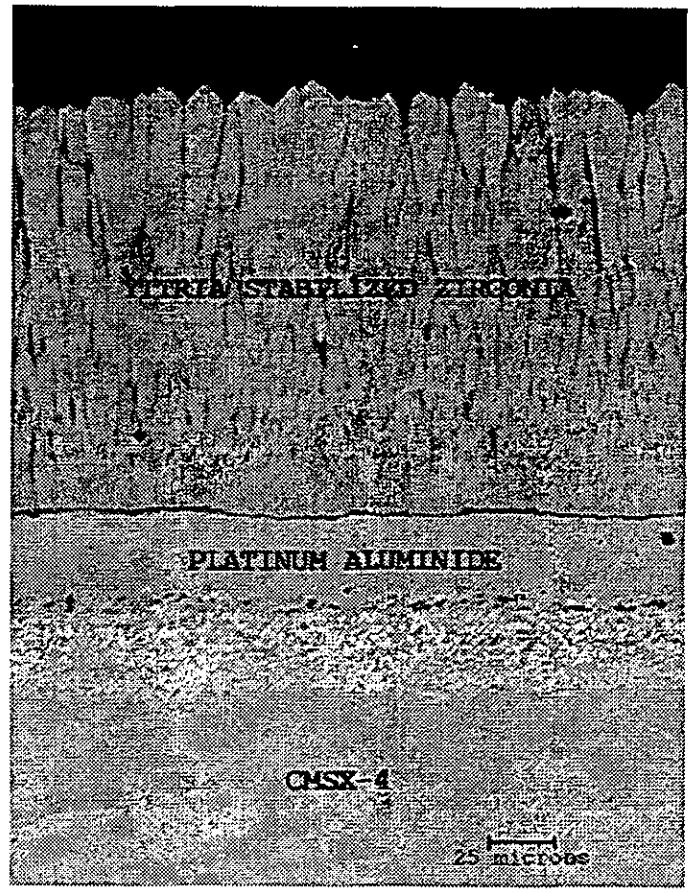


**Fig. 1 - Typical As-Coated Thermal Barrier Coating MicroStructure of a Platinum Aluminide Bond Coat and EB-PVD Deposited Yttria Stabilized Zirconia Top Coat on CMSX-4 Substrate**

in specimen preparation. Coating thickness was measured at 70 microns. A thermally grown alpha ($\alpha$-$Al_2O_3$) is intentionally grown on the platinum aluminide coating to optimize the bond strength of the TBC system. The thermally grown oxide (TGO) is 1 micron thick, and is shown in Figure 2. The yttria stabilized zirconia TBC is applied by the EB-PVD process, which exhibits a columnar structure with gaps or porosity perpendicular to the bond coat interface. The ceramic layer grows outward from the TGO layer in needle-like columns. The EB-PVD thickness is 160 microns on the CMSX-4 alloy shown in Figure 1, and ranged between 170 to 210 microns on the Mar-M 247 alloy.

The microstructure of the EB-PVD TBC coating system on CMSX-10 shows a modified PtAl bond coating, and an identical EB-PVD TBC top coating to the Mar-M 247 and CMSX-4 coating system. The modified platinum aluminide coating exhibits a three layer, two-phase microstructure (Figures 3). The top layer is $PtAl_2$ phases in a Pt-rich NiAl matrix, the intermediate layer consists mainly of Pt-rich NiAl matrix, and the inner layer is the diffusion zone. The total coating thickness was measured at 70 microns. With this particular coating, no topologically close packed (TCP) phases were present. The EB-PVD thickness is 210 microns on the CMSX-4 alloy, with an identical microstructure to the Mar-M 247 and CMSX-4 coating system.

The APS Co-32Ni-22Cr-12Al-0.75Y-1.5Si bond coating, and YSZ-TBC top coating were processed identically for Mar-M247, CMSX-4 and CMSX-10 alloys. Figure 4 shows the representative coating microstructure on CMSX-4. The thickness of the CoNiCrAlY-Si bond coatings range from 150 to 200 microns. The APS YSZ-TBC top coating

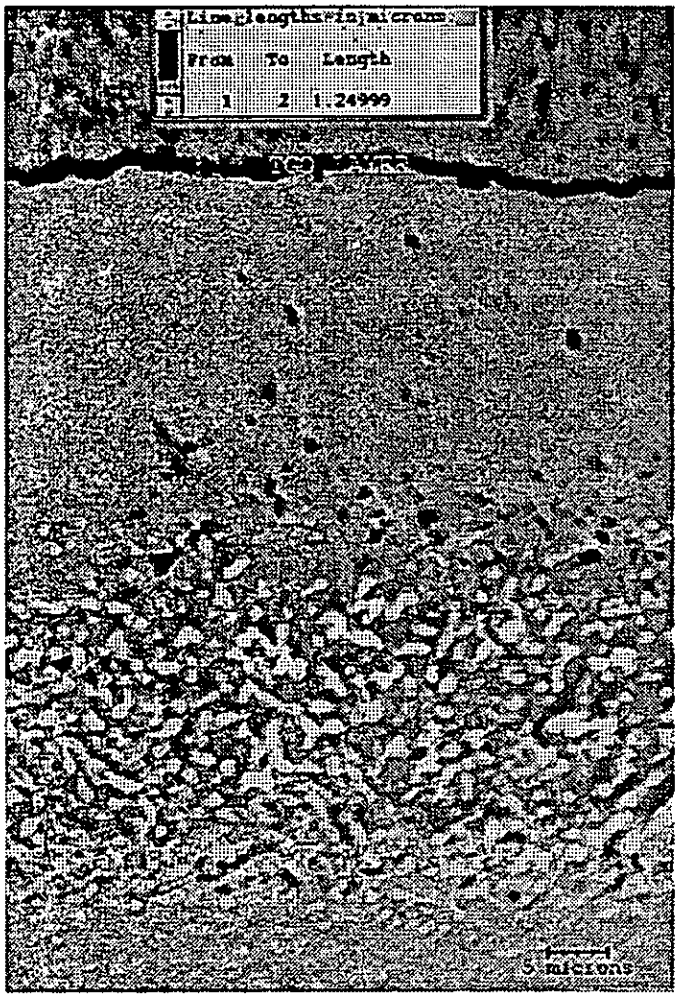


**Fig. 2 - Aluminum Oxide Film Grown at EB-PVD TBC Tope Coat/Platinum Aluminide Bond Coat Interface for CMSX-4 Specien**

typical microstructure displayed in Figure 4 is formed by building up consecutive layers of ceramic, each less than 13 μm thick. The porosity generally appears as equiaxed, round pores that are not linearly connected to one another. The thermal sprayed ceramic top coat thickness ranges from 250 to 300 microns. Thermal spray processes require larger tolerances due to the macroscopic nature of the deposition techniques and rely on rough bond coating surfaces for adequate mechanical adhesion.

Composition. The platinum aluminide bond coatings on Mar-M 247 and CMSX-4 showed some variations, however both coatings exhibited the similar microstructures. The platinum showed 25 wt.% on the Mar-M 247, and only 13 wt.% on the CMSX-4. The aluminum showed similar results with 13 wt.% and 15 wt.% on the Mar-M 247 and CMSX-4 respectively. The higher amount of platinum in the Mar-M 247 alloy may act to improve the stability of the thermally grown oxide. The aluminum concentration is lower than expected for a beta phase NiAl that is between 18 and 35 wt.%. However when using the SEM/EDX technique a lower Al wt.% is usually measured. The platinum aluminide coating on CMSX-10 alloy is a two-phase coating, and therefore exhibits a higher platinum weight percentage. The coating exhibited 32 wt.% platinum and 25 wt.% aluminum. The APS Co-32Ni-22Cr-12Al-0.75Y-1.5Si bond coating had aluminum contents

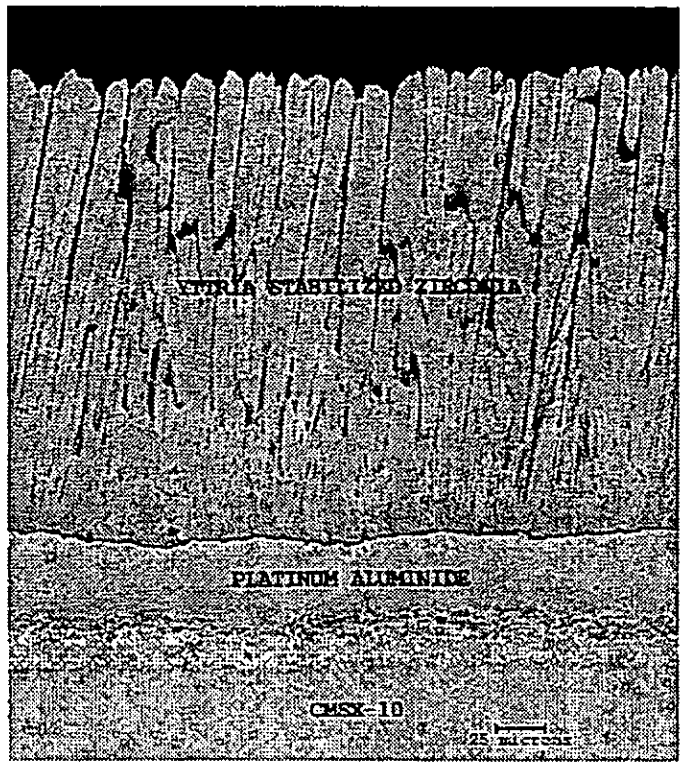


**Fig. 3 - Typical As-Coated Thermal Barrier Coating Microstructure of a Platinum Aluminide Bond Coat and EB-PVD Deposited Yttria Stabilized Zirconia Top Coat on CMSX-10 Substrate**

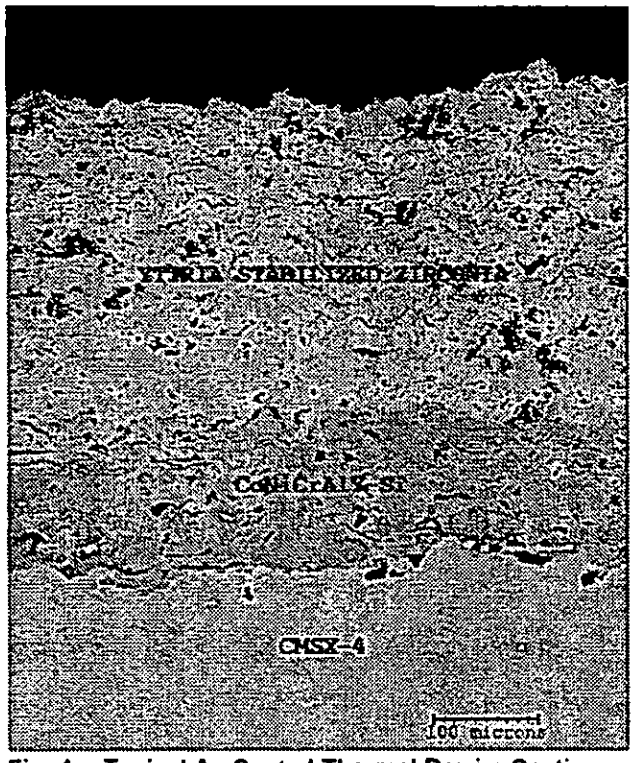


**Fig. 4 - Typical As-Coated Thermal Barrier Coating Microstructure of an Air Plasma Sprayed CoNiCrAlY-Si bond Coat and Yttria Stabilized Zirconia Tope Coat on CMSX-4 Substrate**

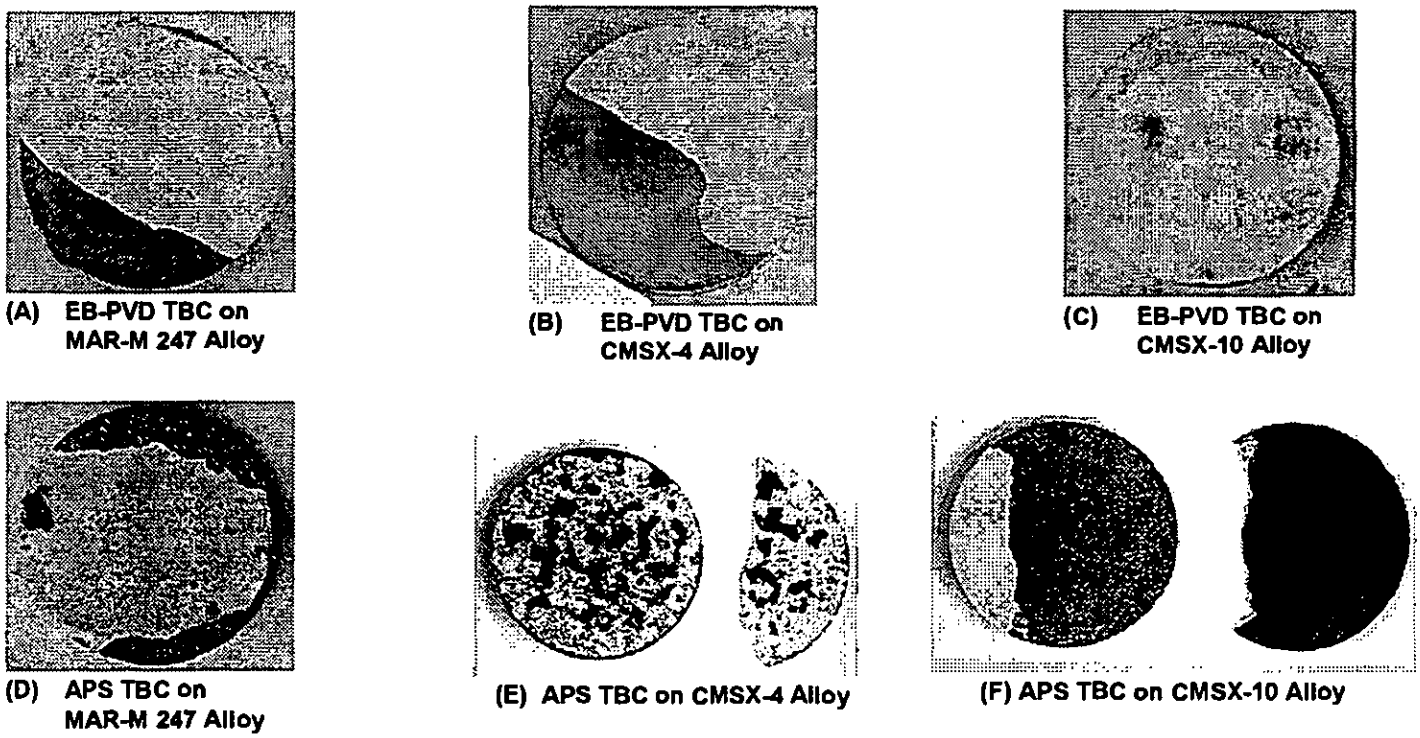


**Fig. 5 - Thermal Cycle Oxidation Test Specimens in Post-Test Condition**

ranging from 8-11 wt.% aluminum at the bond/top coating interface on all alloys. All EB-PVD and APS thermal barrier coatings showed 6-8 wt.% yttria stabilized zirconia.

## 2000°F / 100 hour Thermal Cycles

**Visual Examination**. Figure 5 displays all TBC specimens after thermal cycling. The thermal cycling test was terminated at coating failure or spallation of coating, with the results displayed in Table 2. Failure was determined at the initial stages of ceramic coating spallation. TBC failure ranged from (1) cycle to those that lasted (51) 100-hour cycles. It is interesting to note the obvious failure modes at this point. All the EB-PVD TBC systems showed spallation that initiated at the edges of the specimens, and had different sizes of spallation (Figure 5a,b and c). The TBC had completely separated, suggesting that the spallation occurred at the bond coat-TGO interface. The APS TBC systems showed complete separation of the ceramic on the entire specimen that initiated at the edge of the specimens. The APS TBC on Mar-M 247 and CMSX-4 failed within the ceramic, just above the bond coating. This is represented by the remaining ceramic on the failed coupon (Fig. 5e). The APS TBC on CMSX-10 alloy exhibits a completely blue surface at the debond, representing a failure within the bond coating (Fig. 5f). The EB-PVD and APS TBC specimens all showed failure that initiated at edges due to the coating tensile stresses at the specimen ends. It is evident that TBC life is dependent on many factors including the alloy and bond coating selection, and processing method. These factors will be discussed in detail in the discussion section. After the termination of the cyclic test, the specimens were mounted in epoxy, and sectioned for metallurgical evaluation in order to understand the TBC interfacial behavior after thermal exposure.

**Table 2 – Cycles to Failure For APS and EBPVD TBC Systems. 2000°F FOR 100-Hour Cycles**

| SUBSTRATE ALLOY | EB-PVD TBC | APS TBC |
|---|---|---|
| Mar-M 247 | 12 | 45,51 |
| CMSX-4 | 1,2 | 18 |
| CMSX-10 | 6,7 | 19,26 |

**Microstructure.** The failure of the APS TBC systems occurred within the ceramic approximately 25-50 microns above the bond coating – TBC interface, and the microstructure is shown in Figure 6. The ceramic layer showed a noticeable amount of sintering. The densification of the ceramic layer due to sintering was accompanied by micro-crack formation within the ceramic layer. The micro-cracks act as stress relief sites within the ceramic layer. Severe lateral cracking is also evident in the ceramic that contributed to the failure of the TBC system. An aluminum oxide phase is formed at the interface of the coating that acts as glue in joining the metallic-ceramic system. A pure alumina phase represented by the dark gray areas, and a spinel represented by a light gray phase were formed at the interface. The spinel phase is less stable than the α-alumina and can lead to a failure initiation site. There has been a vast amount of study on the mechanisms that cause the failure in the metallic-ceramic bond on plasma sprayed systems (DeMasi-Marcin, et.al., 1990). The failures shown here relate to the classical case where tensile stresses are generated at the peaks of a bond coating during cooling to room temperature. Cracks are generated at or above these peaks, and cause coating separation based on a combination of crack joining and growth processes. The samples also showed a small degree of delamination at the alloy bond coating interface due to the oxidation of the alloy from the sides of the sample. This is the major failure mechanism in the APS TBC system on CMSX-10 alloy, as shown in Figure 7. CMSX-10

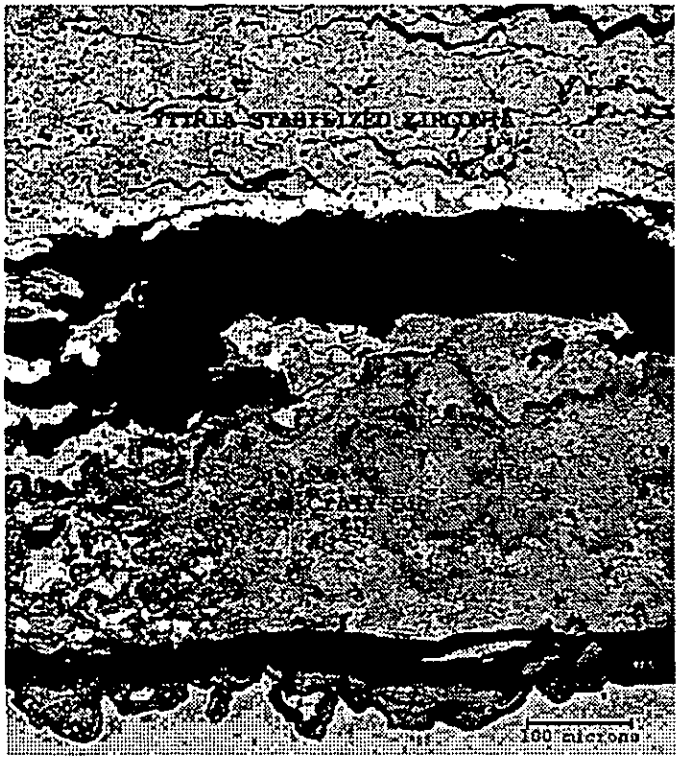


Fig. 6 - Air Plasma Sprayed TBC Microstructure on CMSX-4 Substrate After Thermal Cycle Testing

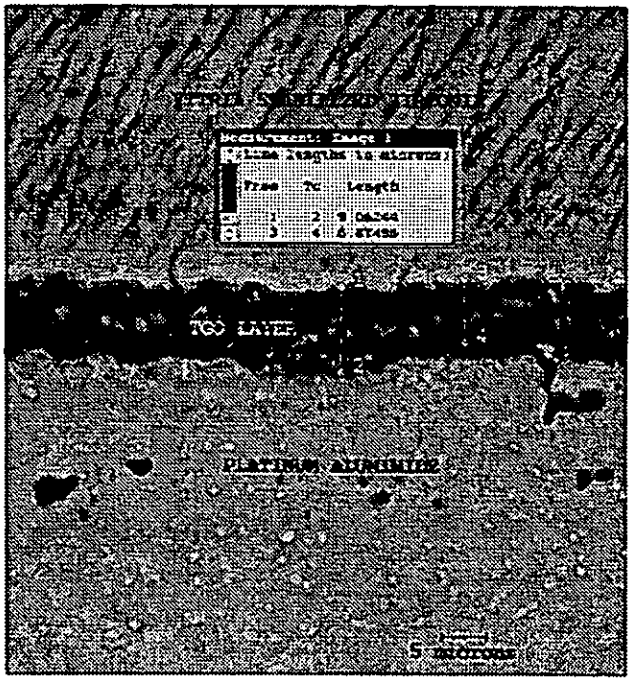


Fig. 8 - Thermally Grown Oxide (TGO) Layer at EB-PVD TBC Top Coat/Platinum Aluminide Bond Coat Interface at the Edge of the CMSX-4 Specimen After Thermal Cycle Testing


Fig. 7 - Air Plasma Sprayed TBC Microstructure on CMSX-10 Substrate After Thermal Cycle Testing

the sides of the sample. This is the major failure mechanism in the APS TBC system on CMSX-10 alloy, as shown in Figure 7. CMSX-10 shows poor oxidation resistance at temperatures above 1800°F (Mutasim, et.al. 1998). The CMSX-10 alloy formed a thick oxide layer that spalled off the bond coating and TBC. The coating also showed a certain degree of cracking within the ceramic and metallic-ceramic interface. It is believed that the sample was close to failure within the ceramic layer based on the microstructure.

The EB-PVD TBC coatings failed at the platinum aluminide-TGO interface. The failures shown are the classic buckling mechanism, and are caused by the stresses on the TGO layer. The stresses can be caused by factors such as roughness at the TGO, sintering of the YSZ, interfacial impurities, and growth stresses of the TGO (DeMasi-Marcin, et.al., 1990). There was no noticeable sintering in the ceramic layer. The EB-PVD ceramic coating on CMSX-4 debonded at the edge of specimen and propagated across the specimen. The thickness and microstructure at the edge and center of the specimen demonstrate this conclusion. The TGO layer at the edge of the specimen (Fig. 8) is a spinel oxide between 7 and 9 microns thick. The combination of the spinel phase that is less stable than the α-alumina, and the high growth stresses at 7-9 microns thickness caused the spallation. The TGO layer in the center of the coating (Fig. 9) is a more stable 3 micron α-alumina layer. It is believed that the low life of the samples (1 or 2 cycles) is related to the processing of the coating. The samples were platinum plated on the ceramic coated side only, leading to excessive oxidation from the sides of the specimen. The CMSX-4 samples will be retested with a platinum aluminide bond coat all over, and the EB-PVD TBC on one side. The EB-PVD TBC samples failed after 6 and 7 cycles, with the microstructure shown in Figure 10. These samples were processed with the bond coat all over and the ceramic coating on one side only. After failure, the TGO layer consists of a 5 micron α-alumina layer.

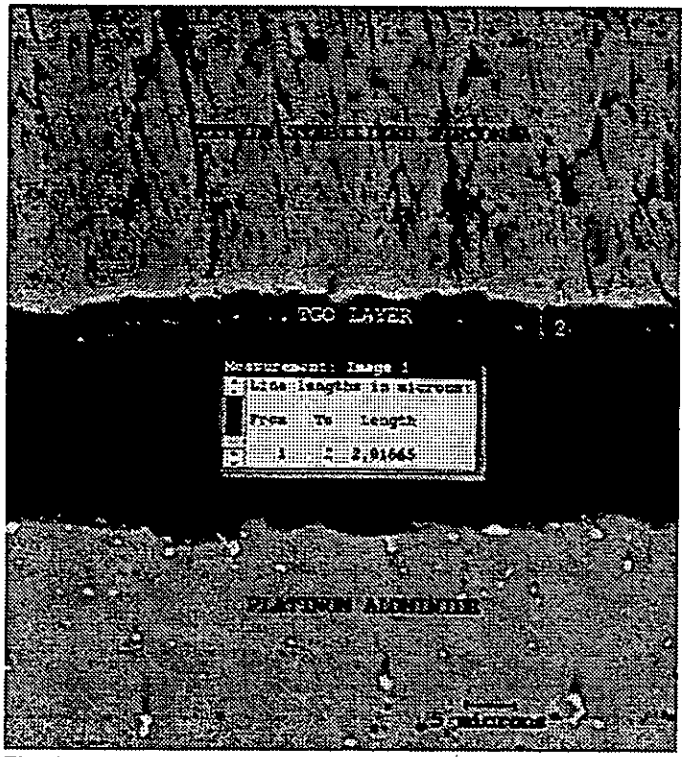


**Fig. 9 - Thermally Grown Oxide (TGO) Layer at EB-PVD TBC Top Coat/Platinum Alluminide Bond Coat Interface at the Center of the CMSX-4 Specimen After Thermal Cycle Testing**

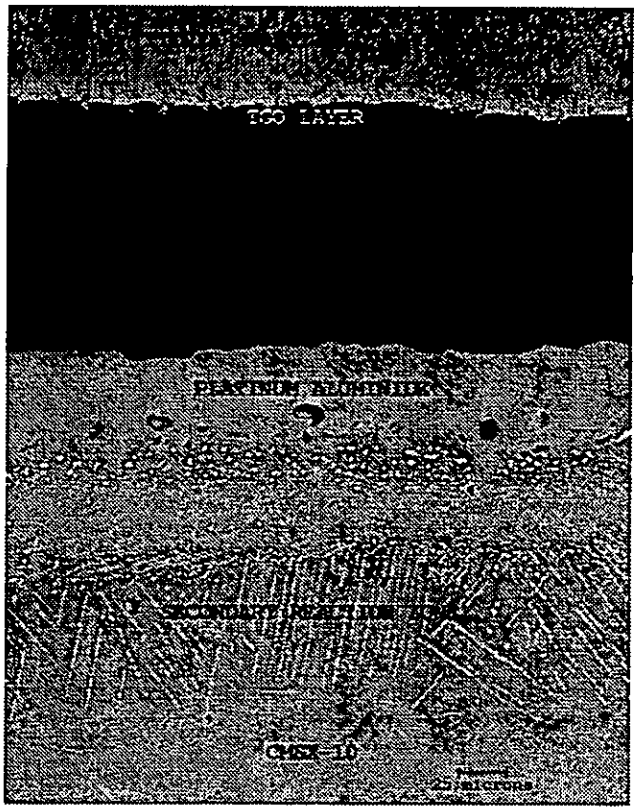


**Fig. 10 - Cross Section of the Platinum Aluminide Bond Coat and EB-PVD Top Coat TBC on CMSX-10 Substrate After Thermal Cycle Testing**

**Table 3. Aluminum Content Versus Cycles to Failure in Bond Coating**

| Coating | Substrate | Al wt.% Before Test | Al wt.% After Test | Cycles to Failure |
|---|---|---|---|---|
| PtAl / EB-PVD TBC | Mar-M 247 | 13 | 11 | 12 |
| PtAl / EB-PVD TBC | CMSX-4 | 15 | 14 | 1,2 |
| PtAl / EB-PVD TBC | CMSX-10 | 25 | 13 | 6,7 |
| APS CoNiCrAlY-Si / TBC | Mar-M 247 | 8 | 1 | 45,51 |
| APS CoNiCrAlY-Si / TBC | CMSX-4 | 8 | 1 | 18 |
| APS CoNiCrAlY-Si / TBC | CMSX-10 | 9 | 1 | 19,26 |

**Composition**. Energy dispersive x-ray analysis was conducted on the oxidized specimens to determine the composition of the various phases in the TBC specimens. The focus was on determining the chemistry of the oxide scales, and the amount of remaining aluminum near the oxide scale. As was clear from the scanning electron micrographs shown in Figures 6 to 10, two oxide scales were identified: pure α-alumina and a mixed oxide layer. The mixed oxide scale (spinel) was identified as (Al,Co,Ni)O which has different thermo-mechanical and physical properties than a-alumina scale. Table 3 lists the aluminum concentrations of the TBC systems before and after the thermal cycle test. A remaining aluminum concentration as low as 1 wt.% was shown for APS TBC system. However, aluminum levels as high as 14 wt.% Al in the platinum aluminide and TBC system resulted in failure.

## DISCUSSION

The performance of thermal barrier coatings is dependent on many factors that include the chemistry and microstructure of the bond and top coatings as well as the process with which the coatings are applied. This study focused on the failure modes and the performance of these coatings. These included the effects of the substrate on the lifetime of an APS and EB-PVD TBC system. The selection of the temperature and cycle time on the lifetime is shown to have a substantial effect.

## APS vs. EB-PVD Thermal Barrier Coating Systems

Two main top coating microstructures were studied. A plasma sprayed coating with equiaxed grains and circular porosity, and an EB-PVD coating with columnar grains and uni-axial porosity. The EB-PVD and APS TBC specimens all showed failure that initiated at edges due to the coating stresses at the specimen ends. The free edge coating stress field demands that the in-plane thermal mismatch stress reduce to zero at the edge of the ceramic. The transition of the in-plane stress to zero causes strong tensile out-of-plane stress along the coating interface (Meier, et.al.,1998). The coating failure mechanisms and a comparison between lifetimes will be discussed.

TBC spallation is a thermo-mechanical phenomenon that results in the formation of cracks within the TBC layers which propagate with time leading to separation of the ceramic from the metallic layer. Bond coating oxidation and build up of cumulative stresses in the TBC system have been identified as the main events that lead to coating spallation (DeMasi-Marcin, et.al., 1990). Two main coating spallation mechanisms were identified in this study. One, which was consistent with the plasma sprayed TBCs, demonstrated failure within the ceramic layer, about 25-50 microns above the oxide/bond coating interface. The second mechanism, which was consistent with the EB-PVD TBCs, showed a planar failure either along or within the oxide layer. These mechanisms are strongly dependent on the type of bonding in each system. The plasma sprayed TBCs depend strongly on the mechanical interlocking between the individual splats in the ceramic coating, and between the ceramic and bond coatings. On the other hand, The EB-PVD TBCs depend on the chemical/metallurgical bonding within the ceramic layer, and between the intentionally thermally grown oxide (TGO) layer and the ceramic top coating. During thermal exposure, a buildup of compressive stresses occurs within the oxide later, and cracks initiate and propagate, and ultimately lead to coating failure. The cracks originate at the weakest location in the TBC system. For plasma spray coatings, this location is usually within the splats near the peaks of the bond coating layer, whereas, it is within the oxide layer of the EB-PVD system.

Tables 2 and 5 shows a clear improvement in the cycles to failure for the APS system over the EB-PVD TBC systems for different temperatures at 100 hour cycle times. The long cycle times in industrial gas turbines have a detrimental effect on the life of EB-PVD TBC systems. EB-PVD TBC systems that lasted 1000 hours in short burner rig cycle times lasted only 90 hours with 10-hour cycles, and only 40 static isothermal hours in furnace tests (Meier, et.al.,1998). The more porous APS system effectively accommodated the stresses created within the TGO and ceramic layers, and resulted in a 2-3 fold lifetime improvement. In addition, the APS system is more tolerant to a thicker oxide scale than the EB-PVD system, and is stable at much lower levels of aluminum (Table 3). The lower levels of aluminum at failure of the APS TBC systems can be attributed to the presence of yttrium and silicon in the bond coating. Yttrium and silicon are expected to improve the chemical stability of the oxide, which is translated to an overall improvement in coating life (Gupta and Duvall, 1986). The higher compliance APS bond coat will not only reduce stresses within the oxide layer, but also reduce thermal stresses within the top ceramic coat, especially when asperities and edges are involved. The EB-PVD system showed only the formation of an $\alpha$-alumina TGO layer up to 5 microns thick, while the APS system showed the formation of varying levels of spinel oxide formation. The presence of spinels and other mixed oxides, which have lower mechanical strengths than $\alpha$-alumina, along the bond/top coating interface would result in increasing the mechanical stresses at the interface and in turn would result in coating failure.

## Effect of Alloy Composition

Table 2 shows a clear improvement in the cycles to failure for the thermal barrier coatings on Mar-M 247 equiaxed alloys versus CMSX-4 and CMSX-10 single crystal alloys. A two-fold improvement was shown for the APS TBCs, and at least a four-fold improvement for the EB-PVD TBC coatings. CMSX-10 alloys exhibit a small increase in cycles to failure over the CMSX-4 alloy; however, more testing is needed to verify this conclusion.

The three alloy compositions are shown in Table 4. Compared to the baseline alloy Mar-M 247, reductions in chromium content were needed to accommodate the increasing addition of rhenium in order to maintain alloy microstructural stability. The variations in the alloy chemistries play an important role in the alloy oxidation performance, their coatability and coating behavior. The change from equiaxed to single crystal alloys with high concentrations of refractory elements brings greater challenges to the coatability and oxidation performance of these alloys. For reference, CMSX-10 alloy contains 19.5 wt.% refractory elements as compared to 16.2 wt.% for CMSX-4 and 15.1 wt.% for Mar-M247 alloy. This variation has a positive impact on the alloy strength, but a negative impact on the coatability and performance of these alloys (Mutasim, et.al.,1998). The decrease in the oxidation performance for the single crystal alloys decreases the stability of the TGO layer therefore decreasing coating life. In addition, the diffusion of refractory elements such as tantalum (Fig. 9, white particles) to the TGO layer has been shown to act as an initiation site for TBC failure. The higher levels of refractory elements, and lower level of chromium in single crystal alloys exhibits a negative impact in coating lifetime.

## Effect of Cyclic Testing Temperature

Thermal cycle testing at 1900°F for 100 hour cycles were conducted on Mar-M 247, CMSX-4, and CMSX-10 samples with the same coatings as described above. The results are shown in Table 5, and clearly display an increase in cycles to failure by decreasing the

**Table 4. Alloy Compositions**

| Alloy | Nl | Co | Cr | Mo | W | Ta | Nb | Al | Ti | Hf | Re |
|---|---|---|---|---|---|---|---|---|---|---|---|
| Mar-M247 | bal. | 10 | 8.4 | 0.7 | 10 | 3 | 0 | 5.5 | 1.1 | 1.4 | 0 |
| CMSX-4 | bal. | 9 | 6.5 | 0.6 | 6 | 6.5 | 0 | 5.6 | 1 | 0.1 | 3 |
| CMSX-10 | bal. | 3 | 2 | 0.4 | 5 | 8 | 0.1 | 5.7 | 0.2 | 0.03 | 6 |

**Table 5. Thermal Cycle Testing Temperature Versus Cycles to Failure**

| Coating | Substrate | 2000°F for 100 Hour Cycles to Failure | 1900°F for 100 Hour Cycles to Failure |
|---|---|---|---|
| PtAl / EB-PVD TBC | Mar-M 247 | 12 | >29 |
| PtAl / EB-PVD TBC | CMSX-4 | 1,2 | >19 |
| PtAl / EB-PVD TBC | CMSX-10 | 6,7 | >34 |
| APS CoNiCrAlY-Si / TBC | Mar-M 247 | 45,51 | >29 |
| APS CoNiCrAlY-Si / TBC | CMSX-4 | 18 | >34 |
| APS CoNiCrAlY-Si / TBC | CMSX-10 | 19,26 | >34 |

**Table 6. Thermal Cycle Testing Time Versus Cycles to Failure**

| Coating | Substrate | 2000°F for 100 Hour Cycles to Failure | 2000°F for 10 Hour Cycles to Failure |
|---|---|---|---|
| APS CoNiCrAlY-Si | Mar-M 247 | 45,51 | 257 |

temperature from 2000°F to 1900°F. The lower testing temperature decreases the rate of bond coating oxidation, and therefore lowers the thickness of the oxide layer, thus increasing the cycle to failure. In a similar study, a comparison of coating life at 2100°F and 1900°F indicated approximately 95% reduction in life for a 200°F increase in exposure temperature (Meier, et.al.,1998).

### Effect of Cycle Time

Thermal cycle testing at 2000°F for 10 hour cycles was only conducted on the APS TBC system on Mar-M 247 alloy. The results are shown in Table 6 and clearly display an increase in cycles to failure, but a decrease of approximately 50% in the total testing time. Mechanical stresses are generated between the metallic and ceramic interface, at or above the TGO layer, during heat-up and cool-down of each cycle due to the thermal expansion mismatch between the various layers. The total cycle time decreased due to increased mechanical stresses on the specimens from cycling. The number of cycles increased because the bond coating oxidation effect is lowered at shorter cycle times.

## CONCLUSIONS

Thermal barrier coating life is very dependent on many factors that include the chemistry and processing of not only the bond and top coatings, but the chemistry of the substrate alloy as well. APS TBCs exhibited a lifetime improvement over EB-PVD TBCs, and the use of single crystal alloys has a negative effect on the TBC lifetimes. The testing parameters also showed a large effect, with increasing temperatures, or decreasing cycle times showing a negative effect on the lifetimes. Even though the APS system has outperformed the EB-PVD system in thermal cycle testing, the strain tolerance provided by the EB-PVD system must be factored into the selection of a TBC system for an engine environment.

## REFERENCES


Bose, S. and DeMasi, J.T., 1995, "Thermal Barrier Coating Experience in Gas Turbine Engine at Pratt & Whitney", Thermal Barrier Coating Workshop, NASA Conference Publication 3312, pp. 63-78.

Brentnall, W.D., Aurrecoechea, J.M., Rimlinger, C.M., Harris, K., Erickson, G.L., and Wahl, J.B., 1997, "Extensive Industrial Gas Turbine Experience With Second Generation Single Crystal Alloy Turbine Blades", International Gas Turbine and Aeroengine Congress & Exhibition. Paper 97-GT-427, Orlando, Florida.

Brindley, W.J. and Miller, R.A., 1989, "TBCs for Better Engine Efficiency", Advanced Materials and Processes 8/89, pp. 29-33.

Broomfield, R.W., Ford, D.A., Bhangu, H.K, Thomas, M.C., Frasier, D.J., Burkholder, P.S., Harris, K., Erickson, G.L., and Wahl, J.B., 1997, "Development and Turbine Engine Performance of Three Advanced Rhenium Containing Superalloys for Single Crystal and Directionally Solidified Blades and Vanes", Presented at the ASME International Gas Turbine and Aeroengine Congress & Exhibition, Orlando, Florida.

DeMasi-Marcin, J.T., Sheffler, K.D., and Bose, S., 1990, "Mechanisms of Degradation and Failure in Plasma-Deposited Thermal Barrier Coating", Journal of engineering for Gas Turbines and Power, vol. 112, pp. 521-522.

Erickson, G.L., 1995, "A New, Third-Generation, Single-Crystal, Casting Superalloy, Journal of Metals, vol. 47, No. 4, pp. 36-39.

Erickson, G.L., 1996, "The Development and Application of CMSX-10", Superalloys 1996, The Minerals, Metals, and Materials Society, pp. 35-43.

Erickson, G.L., 1996, "Unique Single Crystal Superalloys For Industrial Gas Turbine Application", Presented at the Processing and Design Issues in High Temperature Materials, Davos, Switzerland.

Gupta, D.K., and Duvall, D.S., 1986, "Overlay Coatings for Superalloys", U.S. Patent No. Re.32, 121.

Maricocchi, A., Bartz, A., and Wortman, D., 1995, "PVD TBC Experience on GE Aircraft Engines", Thermal Barrier Coatings Workshop, NASA Conference Publication 3312, pp. 79-90.

Meier, S.M., Nissley, D.M., and Sheffler, K.D., 1991, "Thermal Barrier Coating Life Prediction Model Development", Phase II – Final Report, NASA Contractor Report 189111, pp. 47-51.

Mutasim, Z.Z., and Brentnall, W.D., 1995, "Perspective on Thermal Barrier Coatings for Industrial Gas Turbine Applications", Thermal Barrier Coatings Workshop, NASA Conference Publication 3312, pp. 103-112.

Mutasim, Z.Z., Kimmel, J., and Brentnall, W.D., 1998, "Effects of Alloy Composition on the Performance of Diffusion Aluminide Coatings", International Gas Turbine and Aeroengine Congress & Exhibition. Paper 98-GT-401, Stockholm, Sweden.

Mutasim, Z.Z., Rimlinger, C.M., and Brentnall, W.D., 1997, "Characterization of Plasma Sprayed and Electron Beam-Physical Vapor Deposited Thermal Barrier Coatings", International Gas Turbine and Aeroengine Congress & Exhibition. Paper 97-GT-531, Orlando, Florida.

Nelson, W.A. and Orenstein, R.M., 1995, "TBC Experience in Land Based Gas Turbines", Thermal Barrier Coatings Workshop, NASA Conference Publication 3312, pp. 91-102.

Walston, W.S., Ross, E.W., O'Hara, K.S., and Pollock, T.M., 1993, "Nickel-Base Superalloy and Article With High Temperature Strength and Improved Stability", U.S. Patent 5,270,123